Multi-scale imaging at the diamond beamline I13

Cite as: AIP Conference Proceedings **2054**, 030012 (2019); https://doi.org/10.1063/1.5084575
Published Online: 16 January 2019

Christoph Rau, Malte Storm, Shashidhara Marathe, Andrew J. Bodey, Silvia Cipiccia, Darren Batey, Xiaowen Shi, Marie-Christine Zdora, and Irene Zanette

Multi-Scale Imaging at the Diamond Beamline I13

Christoph Rau[1,2,3,*], Malte Storm[1] , Shashidhara Marathe[1] , Andrew J Bodey[1], Silvia Cipiccia[1], Darren Batey[1], Xiaowen Shi[1], Marie-Christine Zdora[1,4], Irene Zanette[1]

[1.] *Diamond Light Source, Harwell Science and Innovation Campus, Didcot, OX11 0DE, UK*
[2.] *University of Manchester, Manchester M1 7HS, UK*
[3.] *Northwestern University, Feinberg School of Medicine, Chicago, Illinois 60611, USA*
[4.] *Department of Physics & Astronomy, University College London, London, WC1E 6BT, UK*

*Corresponding author: christoph.rau@diamond.ac.uk

Abstract The I13 imaging and coherence beamline aims for multiscale imaging in the energy range of 6-30keV. The achievable resolution ranges from several microns to tens of nanometers. Several experimental methods are available on two independently operating branchlines. The Diamond-Manchester imaging branchline applies methods in direct space, such as In-line phase contrast, grating interferometry and full-field microscopy. The coherence branch covers far-field techniques such as ptychography and Bragg-CDI. The ptychography is now available as user-friendly experiment and the spatial and temporal resolution has been significantly enhanced. The scientific program at I13 will increasingly explore the suite of experimental techniques available at the beamline for multi-scale imaging.

INTRODUCTION

The beamline I13 for Imaging and Coherence is one of Diamond's long beamlines with experimental hutches located at about 210m and a total length including the building of about 250m. Details about the instrumentation can be found elsewhere [1,2] and the essential features are briefly summarized here. The beamline is located in one of Diamond's long straight sections. This section has been divided into two smaller 'mini-beta' sections, hosting two canted undulators and small ID gaps increasing the flux by an order of magnitude compared to a standard long straight section. The insertion devices can be operated independently, and subsequently one beamline branch is dedicated to imaging in real space ('Imaging' or Diamond-Manchester Imaging Branchline) the other –the Coherence branch- to imaging in reciprocal space. Different techniques combined permit to cover a large range in spatial resolution from a couple of microns down to currently tens of nanometers.

DIAMOND-MANCHESTER IMAGING BRANCHLINE

The imaging branchline covers the resolution range from about 5 microns to 50nm. For user operation mostly In-line phase contrast tomography is used, grating interferometry and full-field microscopy are currently under development and open for friendly user mode.

In-line phase contrast tomography

In-line phase contrast imaging provides micrometer resolution and is mainly applied for studies on samples with weak contrast or in-situ and in-operando studies. In pink-beam mode scanning times are typically some minutes for a complete tomography, but can be reduced also to seconds, if required. The pink beam is generated by the combination of X-ray filters and the coated X-ray mirror, filtering some few undulator harmonics out of the undulator spectrum [3]. For element specific experiments a multilayer monochromator (MLM) or a double crystal monochromator (DCM)

Proceedings of the 13th International Conference on Synchrotron Radiation Instrumentation – SRI2018
AIP Conf. Proc. 2054, 030012-1–030012-6; https://doi.org/10.1063/1.5084575
Published by AIP Publishing. 978-0-7354-1782-3/$30.00

can be used. Today for most experiments pink beam is used, the MLM is important for the TXM and grating interferometry reducing significantly the recording times.
Experiments with customized sample environments are carried out on large variety of scientific questions, such as the study of dissolving CO_2 in brine and sandstone, the study of battery failure, micro-cracks in nuclear materials or even the properties of ice-cream depending on their history (an overview can be found in [18]).

Monochromator	Materials	Energy range	Energy bandwidth	Reflectivity
DCM	Si(111)	6-35 keV	$1.4*10^{-4}$	95%
MLM	V / B_4C	20-39 keV	0.5% @ 30keV	89% @ 30keV
	Ru / B_4C	6-22 keV	4.7% @ 10keV	79% @8.05keV
	Mo / B_4C	8-22 keV	0.7% @ 10keV	72% @8.05keV

TABLE 1. Characteristics for imaging branch monochromators (calculated).

Grating interferometry

Grating interferometry provides outstanding image quality, especially for samples with weak absorption contrast. The methods permits quantifying phase shift along the sample and detecting small-angle scattering within sample features. Because the phase information is by about two orders of magnitude more sensitive in the given energy range of the beamline, data segmentation is simplified [6], see figure 1. The dark field information helps distinguishing materials with similar absorption but different small angle scattering properties.

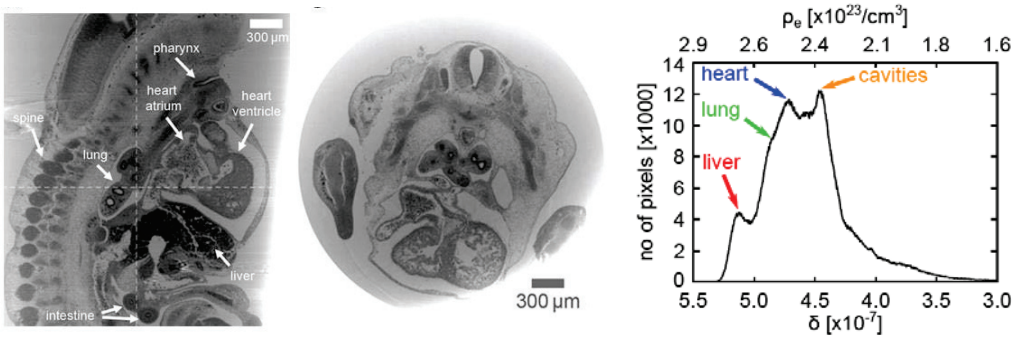

FIGURE 1. Example for tomography with grating interferometry. Sagital and axial sections of a 3D phase tomography reconstruction mouse embryo sample (left and centre) and histogram with phase information (right). Different organs can be distinguished in the histogram [6].

For the I13 setup (in preparation), the samples is suspended below the rotation stage in a liquid filled bath for avoiding artefacts for the phase reconstruction at the sample interface (see figure 2). The interferometer can be either operated with a single or a double grating. Several phase gratings for energies of 14, 19 and 30 keV, a period of 4.8µm and with π/2 or π phase shifts will be used, the π phase shift grating in junction with a 2.4µm absorption grating for the double grating interferometer. The MLM provides sufficiently limited energy bandwidth and reduces the recording times to some 100ms per projection.

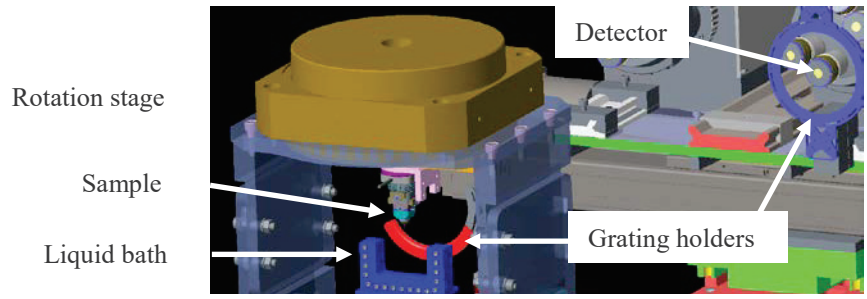

FIGURE 2. Scheme for grating interferometry setup. The sample is located beneath the rotation stage and can reside in a bath filled with liquid. The bath is covered with capton foils (not shown).

Full-field microscope

The full-field microscope provides about 50-100nm spatial resolution over a large field of view of about 50-100 microns [4]. The large working distance of several centimeters enables the implementation of dedicated sample environments. The detector is located about 8m from the sample stage. A beam shaper optic is used as condenser, adapting the field of view of the instrument to the experimental requirements. The field of view is about 50-100 microns, depending on the photon energy, and is matched to the depth of field of the objective lens. Fresnel zone plates are chosen as objective lens and with an outermost zone width of 50-150nm they provide a resolution of 75-200nm [5]. Their large working distance/long focal length of about 50-100mm provides space for dedicated sample environments. For weakly absorbing samples, phase rings are installed in the back focal plane for positive and negative Zernike phase contrast. The Hamamatsu C12849-101U detector provides high photon efficiency with an effective pixel size of 6 microns. It has been recently demonstrated that the multilayer with a relatively large energy bandwidth (compared to the requirements of the zone plates) can be used for the microscope. This –together with the use of the medium resolution detector- the recording times are currently in the order of some hundred milliseconds. This reduces the scanning times for a complete tomographic scan to about 30 minutes and even less. In the near future it is planned to place the instrument on a table further upstream at a distance of about 13m from the detector and to increase the user-friendliness of the instrument for full implementation into the user program.

In figure 3 a typical scientific application with the instrument is shown. Here the thermal long-term stability of photonic glass, fabricated from Zirconia ceramic beads with 2µm diameter is studied. The material, pre-calcinated at 700°C for 3h, (left) deteriates after further calcination a at 1400°C for 192h. The beads collapse after the treatment and loose their infra-red reflective properties.

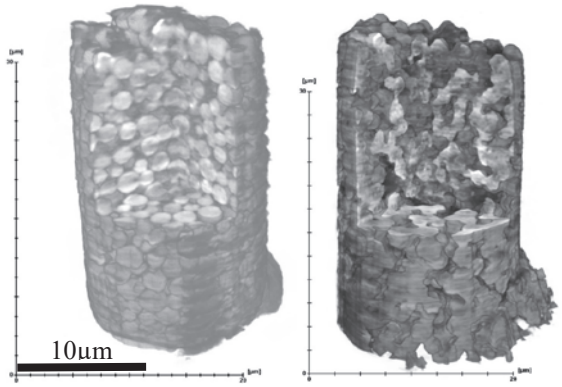

FIGURE 3. TXM measurement of photonic crystals consisting of Zirconia beads before (left) and after (right) thermal treatment.

COHERENCE BRANCHLINE

The coherence branch performs imaging in reciprocal space, mainly ptychography and Bragg- CDI, also coherence related experiments such as holography, XPCS, and optics characterization. The scheme for the branchline layout is shown in fig. 5.

Ptychography

The ptychography experiment completes the imaging branch techniques in terms of resolution. High-efficiency zone plates can focus the beam to a size of about 50nm. With maximum detector to sample distance of about 14m, the optic can be defocused to up to about 20µm. Currently the SmarAct translations stages can be reliably scanned with 20Hz frequency in step scan mode and dedicated software [8,9]. Using pink beam [3,10,11] we most recently demonstrated 18nm spatial resolution and 1ms exposure times and slightly reduced resolution with 100µsec exposure times (see figure 4). This result -together with some equipment upgrade- will allow us reducing the recording times for tomography scans from currently typically 3-6 hours to some minutes and eventually even less.

The integration of user-friendly GUI based software for controlling the experiment and the ‘pycho’ software for data-analyses makes the technique accessible for general user operation.

More details about the ptychography experimental station can be found in the present proceedings [12]. The ptychography setup is complemented with some fluorescence measurement capabilities, again more details about the equipment and software can be found elsewhere [12,13].

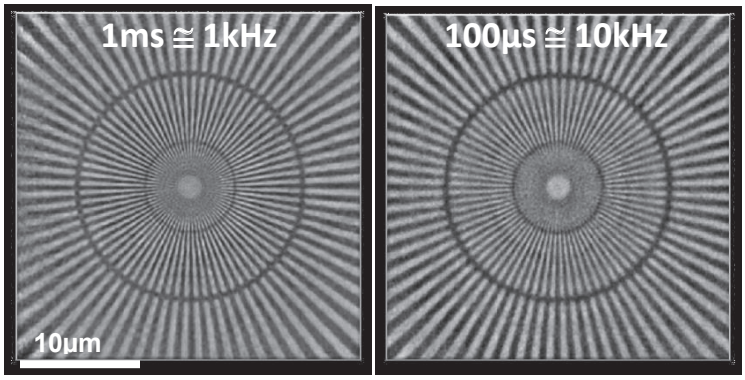

FIGURE 4. Reconstructed test pattern with pink-beam ptychography and t_{exp}=1ms (left) and t_{exp}=100µs (right).

Bragg-CDI

Currently Bragg-CDI and ptychography share the same focusing optics and sample stages. For Bragg-CDI a combination of two robot arms is used to hold vacuum tube and detector. The robot arms drift by some microns (<4µm in after thermalisation), keeping the thermal environment stable by +-0.2 degrees [14]. The detector can be placed at a maximum distance of about 8m from the sample, the angular range is currently 30degress horizontally and 28degrees vertically and may be further extended. Mostly Bragg-CDI is applied for investigating the stress within nano-crystals, as for example for the photo-induced structural changes in BiFeO3 nanocrystals [15].

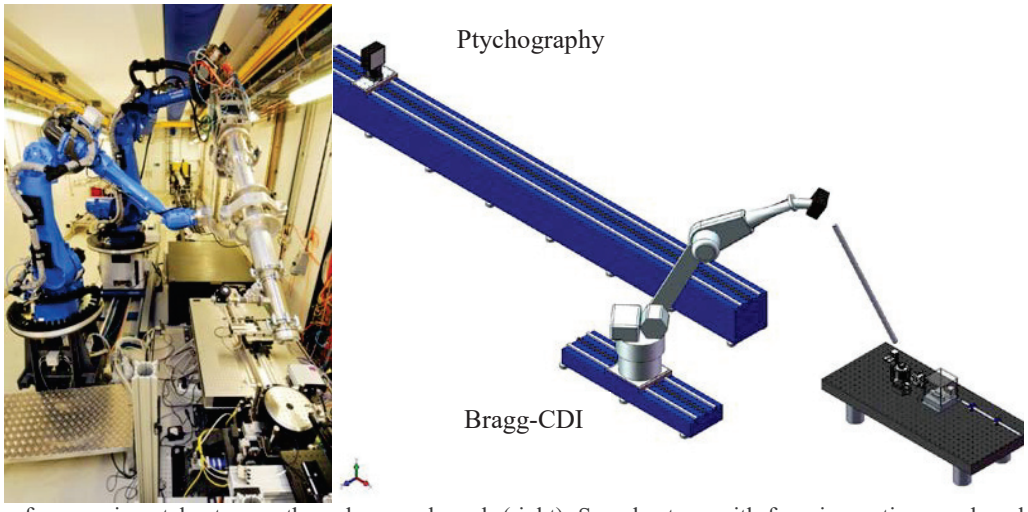

FIGURE 5. Scheme for experimental setup on the coherence branch (right). Sample stage with focusing optics are shared for ptychography and Bragg-CDI. Two robot arms are used for Bragg-CDI (left) a long translation rail for ptychography.

Detector

For ptychography and Bragg-CDI mainly the in-house developed EXCALIBUR detector is used [16]. The device is based on the MediPIX3 chip with an 256x256 array and 55 microns pixel size. Three modules with 2x8 chips are assembled for the detector providing an array of 2048x1526 pixels. The detector can be operated in back-to-back mode at 12bit image depth, and in 24bit mode. Originally the detector was designed for 100Hz readout in continuous mode and 1kHz, nowadays 250Hz continuous readout is achieved and will be improved further.

Data analyses

For tomography experiment, data can be reconstructed during the experimental visit. There exist 3 clusters for processing tomography data. These clusters make use of 3 generations of NVIDA graphics cards, M2070, K80 and P100 cards. Each cluster has around 10 nodes in it each of which has 2 Graphics Cards from one of the generations. The GPU clusters are generally refreshed every 2 years. The ptychography data can currently be reconstructed within 10minutes for an array with 1024 points and a 512x512 detector pixel array and will be reduced further with specific GPU based acceleration software. It is expected that at the end of each experiment full 3D data sets have been reconstructed. For further data analyses users can return to the facility in the same way as for the experiment itself. A schedule is produced for data analyses visits on site and making use of the Diamond infrastructure. Different software packages are available such as Avizo, the computers have the following specification and are continouisly upgraded: 512GB DDR 4 RAM, dual Intel Xeon E5 - 2687W v3 CPUs (3.1GHz, 10 cores, 20 threads), dual NVIDIA Quadro K6000 GPUs with 12GB GDDR5 RAM and ECC, dual 512GB SSDs in RAID 1, 10Gbs-1optic fibre connections and 30-inch monitors. For more details see [17].

Examples for Multi-scale imaging

Many scientific questions require -in terms of spatial resolution- investigating structures and properties over several orders in magnitude. This is the case for example dendritic growth of metals, the generation of cracks in materials or the origins of battery failure. In biology -between many other other examples- for moth wings the mechanical properties are given by their micro- and nano-structure.

Many research problems are initially investigated on the micron lengthscale. In the following the study progresses with increased resolution finally on the results with highest spatial resolution are achieved on the coherence branchline.

SUMMARY

A suite of instruments available enabling multi-scale imaging in energy range 6-30keV and resolution microns to tens nanometers. The diverse capabilities are listed in the table below.

Branchline	Imaging	Imaging	Imaging	Coherence	Coherence
Method	In-line phase contrast	Grating Interferometry	Full-field microscope	Ptychography &Fluorescence	Bragg-CDI
Status	Operational	First users	First users	Operational	First users
Energy	8-30keV	14-25keV	8-13keV	6-20keV	6-20keV
Field of view (baseline)	1-14mm	1-14mm	50-100µm	55-110µm	~µm
Resolution 2D	1-5µm	>5µm	50-200nm	18-200nm	50nm
Exposure time	100µs	>200ms	>200ms	100µs-50ms	10s
Resolution 3D	2µm	>5µm	>100nm	>100nm	50nm
Tomoscan	4s-10min	<4h	10min	3-6h	3-6h

TABLE 2. Summary of Beamline I13 imaging capabilities.

Acknowledgements

The I13 beamline is supported for construction and operation of the Diamond-Manchester branchline by the Diamond-Manchester collaboration. Ulrich Wagner contributed to the beamline construction and the implementation of advanced beamline optics. The beamline collaborates with the team of Christian David for the fabrication and implementation of X-ray optics, Jeroen Bosgra and Florian Doering are acknowledged for their contributions in particular. Kazimir Wanelik and Andrew Williams are acknowledged for their relentless support for the beamline software and controls. J.J. do Rosario (TUHH) and E. W. Leib (Univ. HH) provided samples to Malte Storm for the TXM measurements.

REFERENCES

[1] C. Rau, U. Wagner, Z. Pešic, and A. De Fanis, Physica Status Solidi (a) **208**, 2522 (2011).
[2] C. Rau, Synchrotron Radiation News **30**(5), 19 (2017).
[3] C. Rau, T. Weitkamp, A. A. Snigirev, C. G. Schroer, B. Benner, J. Tuemmler, T. F. Guenzler, M. Kuhlmann, B. Lengeler, C. E. Krill, K. Doebrich, D. Michels, A. Miches, *Proc. SPIE, Developments in X-Ray Tomography III,* 2002*,* edited by U. Bonse (SPIE, 2002), Vol. 4503, pp. 9.
[4] J. Vila-Comamala, J. Bosgra, D. S. Eastwood, U. Wagner, A. J. Bodey, M. Garcia-Fernandez, C. David and C. Rau, *Proceedings of the 12th International Conference on X-Ray Microscopy*, 2016, edited by M. D. de Jonge, D. J. Paterson and C. G. Ryan, (AIP Conf. Proc., 2016) Vol. 1696, p. 020036.
[5] K. Jefimovs, Konstantins , J. Vila-Comamala, M. Stampanoni, B. Kaulich, and C. David, J. Synchrotron Rad. **15, 106** (2008).
[6] M. C. Zdora, J. Vila-Comamala, G. Schulz, A. Khimchenko, A. Hipp, A. C. Cook, D. Dilg, C. David, C. Grünzweig, C. Rau, P. Thibault, and I. Zanette, Biomed. Opt. Express **8**, 1257 (2017).
[7] S. Marathe, M. C. Zdora, I. Zanette, S. Cipiccia, and C. Rau, *Proc. SPIE, Developments in X-Ray Tomography XI,* 2017, edited by B. Müller and G. Wang (SPIE, 2017), Vol. 10391.
[8] D.A. Sherrell, A. J. Foster, L. Hudson, B. Nutter, J. O'Hea, S. Nelson, O. Paré-Labrosse, S. Oghbaey, R. J. D. Miller, and L.R. Owen, *J.* Synchrotron Rad. **22**, 1372 (2015).
[9] R. L. Owen, D. Axford, D. Sherrell, A. Darren, A. Kuo, O. P. Ernst, E. C. Schulz, R. J. D. Miller, H. M. Mueller-Werkmeister, Acta Cryst. **D73**, 373 (2017).
[10] T. B. Edo, D. J. Batey, A. M. Maiden, C. Rau, U. Wagner, Z. D. Pešic, T. A. Waigh, and J. M. Rodenburg, Phys. Rev. A **87**, 053850 (2013).
[11] D. J. Batey, T. B. Edo, C. Rau, U. Wagner, Z. D. Pešic, T. A. Waigh, and J. M. Rodenburg, Phys. Rev. A **89**, 043812 (2014).
[12] S. Cipiccia, D. Batey, X. Shi, S. Williams, K. Wanelik, A. Wilson, P. Martin, T. Scott, and C. Rau, *Proceedings SRI2018*, Taiwan 2018, edited by Shangjr Gwo, Di-Jing Huang, and Der-Hsin Wei, (AIP Conf. Proc. 2018) (accepted).
[13] S. Cipiccia, D. Batey, X. Shi, S. Price, A. Parsons, K. Wanelik, A. Wilson, R. Crook, R. Raja, and C. Rau, 'An Iterative algorithm for self-absorption correction in 3D fluorescence imaging', Microscopy and Microanalysis, 24, S2, 94-95 (2018).
[14] Z. D. Pešic, A. De Fanis, U. Wagner, and C. Rau, *Proceedings SRI2012*, Lyon 2012, (J. Phys.: Conf. Ser. 2013), Vol. 425, p. 182003.
[15] M. Newton, A. Parsons, U. Wagner, and C. Rau, New *J.* of Physics **18**, 093003 (2016).
[16] N. Tartoni, G. Dennis, P. Gibbons, E. Gimenez, I. Horswell, J. Marchal, U. Pedersen, Z. Pešic, R. Plackett, C. Rau , R. Somayaji, J. Spiers, J. Thompso, B. Willis , C. Angelsen , P. Booker, S. Burge, J. Lipp , T. Nicholls, S. Taghavi, and M. Thorpe, *IEEE Nuclear Science Symposium and Medical Imaging Conference Record* (NSS/ MIC) N2-003 (IEEE 2012) pp 530-533.
[17] A. J. Bodey and C. Rau, Proceedings XRM 2016, Oxford 2016, (J. Physics: Con. Ser. 2017), Vol. 849(1), p. 012038.
[18] C. Rau, A. Bodey, M. Storm, S. Cipiccia, S. Marathe, M. C. Zdora, I. Zanette, U. Wagner, D. Batey, X. Shi, *Proc. SPIE, Developments in X-Ray Tomography XI,* 2017, edited by B. Müller and G. Wang (SPIE, 2017), Vol. 10391.